PCCP

PAPER

View Article Online
View Journal | View Issue

Cite this: *Phys. Chem. Chem. Phys.*, 2014, **16**, 2499

Correlations between lithium local structure and electrochemistry of layered $LiCo_{1-2x}Ni_xMn_xO_2$ oxides: ^{7}Li MAS NMR and EPR studies

Radostina Stoyanova,*[a] Svetlana Ivanova,[a] Ekaterina Zhecheva,[a] Ago Samoson,[b] Svetlana Simova,[c] Pavleta Tzvetkova[c] and Anne-Laure Barra[d]

Received 20th October 2013,
Accepted 27th November 2013

DOI: 10.1039/c3cp54438a

www.rsc.org/pccp

Advanced ^{7}Li MAS NMR technologies and high frequency EPR are combined to identify structural motifs and their relation to electrochemical properties of layered lithium–cobalt–nickel–manganese oxides $LiCo_{1-2x}Ni_xMn_xO_2$ ($0 < x \leq 0.5$) used as cathode materials in lithium ion batteries. Structural–chemical shift regularities were established by systematic variation of the ratio of diamagnetic Co^{3+} to paramagnetic Ni/Mn ions with variable valences. While EPR allows identifying the oxidation state of transition metal ions inside the layers, ^{7}Li NMR probes the local structure of Li with respect to transition metal ions located in two adjacent layers. For assignment of the lithium chemical shifts, we examine first magnetically diluted $LiCo_{1-2x}Ni_xMn_xO_2$ with $x = 0.02$, where paramagnetic ions are stabilized only in Mn^{4+} and Ni^{3+} form. Then the studies are extended towards the intermediate compositions with $x = 0.10$ and 0.33, containing simultaneously paramagnetic Mn^{4+}, Ni^{3+} and Ni^{2+} ions and diamagnetic Co^{3+} ions. The benefit of using NMR with ultrafast spinning rates is demonstrated for the end composition $LiNi_{0.5}Mn_{0.5}O_2$ having only paramagnetic Ni^{2+} and Mn^{2+} ions. The local structure of Li is quantified in respect of the number of Ni^{2+} and Mn^{4+} neighbors. It has been demonstrated that Ni^{2+} and Mn^{4+} are non-randomly distributed around Li and their distribution depends on the method of synthesis. The extent of local cationic order and its effect on the electrochemical properties of $LiNi_{0.5}Mn_{0.5}O_2$ are discussed.

Introduction

Linking the electrochemical properties of layered oxides with the local structure of lithium is a key topic in the field of lithium ion batteries due to its high potential to design more effective electrode materials.[1,2] Recently, lithium–cobalt–nickel–manganese oxides, $LiCo_{1-2x}Ni_xMn_xO_2$, with compositions $x = 1/2$ and $x = 1/3$ were proposed as next generation electrode materials.[3,4] Contrary to the conventional $LiCoO_2$-based electrodes, $LiCo_{1-2x}Ni_xMn_xO_2$ oxides display two electron electrochemical reactions during reversible lithium intercalation, a phenomenon that is generally considered to be rare for layered oxides.[4]

To improve the electrochemical performance of $LiCo_{1-2x}Ni_xMn_xO_2$, a detailed knowledge of the oxidation state and the local structure of transition metal ions is needed. In general, $LiCo_{1-2x}Ni_xMn_xO_2$ has a structure composed of discrete layers of lithium and transition metal ions.[3,4] When several transition metal ions coexist in the layers, the identification of their oxidation state, as well as the determination of their local structure, becomes a difficult task. In this context, electron paramagnetic resonance spectroscopy (EPR) working at higher frequency and stronger magnetic fields is best suited for direct observation of the electronic and coordination geometry of paramagnetic ions.[5] Recently, we have demonstrated the capability of high-frequency EPR for analysis of the oxidation state and local structure of nickel, manganese and cobalt ions in layered $LiCo_{1-2x}Ni_xMn_xO_2$ with x varying in the whole concentration range ($0 \leq x \leq 0.5$).[6–9] It has been found that the nickel and manganese ions substitute for diamagnetic Co^{3+} in the CoO_2-layers and stabilized as Ni^{3+}, Ni^{2+} and Mn^{4+}.[8,9] The local structure probed by EPR encompasses the transition metal ion in a trigonally distorted octahedron extended by the first 6 transition metal ions inside the layers (Fig. 1). When $x \geq 0.33$, a new phenomenon is established: there is a local non-homogenous distribution of Ni^{2+} and Mn^{4+} inside the transition metal layers without perturbing the long-range

[a] *Institute of General and Inorganic Chemistry, Bulgarian Academy of Sciences, 1113 Sofia, Bulgaria. E-mail: radstoy@svt.igic.bas.bg; Fax: +359 2 8705024; Tel: +359 2 979 3915*
[b] *Tehnomeedikum, Tallinn University of Technology, Estonia*
[c] *Institute of Organic Chemistry with Centre of Phytochemistry, Bulgarian Academy of Sciences, 1113 Sofia, Bulgaria*
[d] *Laboratoire National des Champs Magnétiques Intenses, CNRS, 38042 Grenoble Cedex 9, France*

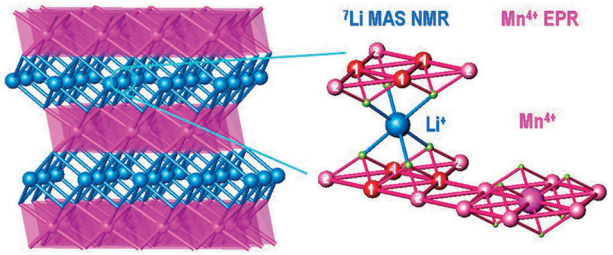

Fig. 1 Schematic representation of the transition from the long-range structure of $LiCo_{1-2x}Ni_xMn_xO_2$ to the local structures of Li and transition metal ions that can be probed by the ^{7}Li NMR and EPR, respectively. Blue, red and green colours correspond to lithium, transition metal ions and oxygen. The 90° and 180° bounded Mn^{4+}/Ni^{n+}–O–Li^+ configurations (1 and 2 positions, respectively) are given by big and small balls.

crystal structure.[10] The extent of non-homogeneous distribution is sensitive towards the method of synthesis.[11]

The cationic distribution of the transition metal ions has also an impact on the lithium mobility in the lithium layers and, in turn, on the electrochemical properties of $LiCo_{1-2x}Ni_xMn_xO_2$. In this context, the properties of $LiCo_{1-2x}Ni_xMn_xO_2$ can be optimized if we are able to probe the local structure of lithium by NMR.[12–18] When Li^+ is located in the environment created by diamagnetic ions such as Li^+ and Co^{3+} the main resonance appears at around 0 ppm.[12,19] The appearance of the paramagnetic ions in close proximity to Li^+ leads to a shift of the resonance outside the region typical for diamagnetic shifts.[20] In this case, the important piece of information comes from the interactions between the Li nucleus and an unpaired electron of Ni and Mn ions.[12,15] Based on the hybrid density functional theory calculations, it has been demonstrated that the lithium chemical shift in the paramagnetic layered oxides such as $LiNiO_2$ and $LiCo_{1-x}Ni_xO_2$ can be examined using a simple structural model including the distinct lithium–oxygen–transition metal bond pathway contributions.[21] In the layered structure, two types of Li^+–O^{2-}–Ni/Mn^{n+} configurations with bond angles of 90° and 180° are mainly responsible for the observed chemical shift, while interactions beyond these configurations are insignificant (Fig. 1). Detailed ^{6}Li NMR studies of $LiCoO_2$, $LiCo_{1-x}Ni_xO_2$ and $LiNi_{0.5}Ti_{0.5}O_2$ allow us to quantify the shift of ^{6}Li caused by paramagnetic Mn^{4+}, Ni^{2+} and Ni^{3+} ions:[12,16,17,22] +250 and −60 ppm for 90° and 180° bounded Mn^{4+}–O–Li^+ ions, respectively; −30 and +170 ppm for 90° and 180° Ni^{2+}–O–Li^+ configurations, and −15 and +110 ppm for 90° and 180° Ni^{3+}–O–Li^+ configurations. Due to the smaller quadrupole moment of ^{6}Li, its NMR spectra are better resolved as compared to the ^{7}Li ones, but the lower natural abundance (~7%) requires, for practical application, an isotopic enrichment of the oxides with ^{6}Li. This has been demonstrated for $LiCoO_2$ slightly doped with nickel and manganese.[17] Although the effects of paramagnetic ions on ^{6}Li NMR spectra are well described for layered oxides with low and intermediate concentration of paramagnetic ions,[12,17,18] the local structure of lithium in more concentrated oxides remains unexplored. This is a consequence of the experimental difficulties connected with the use of fast magic spinning rates needed to suppress the magnetic interactions. In addition, the exact identification of the oxidation states of transition metal ions in $LiCo_{1-2x}Ni_xMn_xO_2$ and their relationship with the local environment of Li are still under debate.

The aim of this contribution is to access the local structure of Li nucleus in layered $LiCo_{1-2x}Ni_xMn_xO_2$ oxides going from a diamagnetic to a paramagnetic state ($0 < x \leq 0.5$) by using solid state ^{7}Li NMR with adequate magic angle spinning. The analysis of all ^{7}Li MAS NMR spectra is based on high-frequency EPR data on the oxidation states of nickel and manganese ions in double substituted oxides $LiCo_{1-2x}Ni_xMn_xO_2$. Therefore, we examine first magnetically diluted $LiCo_{1-2x}Ni_xMn_xO_2$ with $x = 0.02$, where only Mn^{4+} and Ni^{3+} are stabilized. Then the studies are extended towards the intermediate compositions with $x = 0.10$ and 0.33, containing simultaneously paramagnetic Mn^{4+}, Ni^{3+} and Ni^{2+} ions and diamagnetic Co^{3+} ions. Finally, the end composition $LiNi_{0.5}Mn_{0.5}O_2$ containing only paramagnetic Ni^{2+} and Mn^{2+} ions are investigated. To demonstrate further the potential of ^{7}Li NMR we compare the local environment of Li in two different $LiNi_{0.5}Mn_{0.5}O_2$ compositions with good and worse electrochemical properties.

Experimental

$LiCo_{1-2x}Ni_xMn_xO_2$ samples were prepared by the co-precipitation method as described elsewhere.[8–10] This method relies on a solid state reaction between mixed Co, Ni, and Mn oxides with lithium hydroxide at 950 °C. Mixed Co, Ni, and Mn oxides are obtained by thermal decomposition of co-precipitated Co, Ni, and Mn carbonates. To compensate for the lithium volatility, an excess of 2% $LiOH{\cdot}H_2O$ was used. For the end composition $LiNi_{0.5}Mn_{0.5}O_2$, two types of precursors are applied: $Ni_{1.5}Mn_{1.5}O_4$ with a spinel-type structure and $NiMnO_3$ with an ilmenite-type structure. The solid state reaction proceeds for both precursors at 900 °C.[10]

X-ray structural analysis was performed using a Bruker Advance 8 diffractometer with CuKα radiation. Step-scan recordings for structure refinement by the Rietveld method were carried out using 0.03° 2θ steps of 10 s duration. The computer program FULLPROF was used in the calculations.[23] In agreement with previous structural characterization,[8–10] the structural model used comprised Li in 3b sites (0 0 0.5), $Co_{1-2x}Ni_xMn_x$ in 3a sites (0 0 0) and oxygen in 6c sites (0 0 z) for the R-3m space group. The functional Li/(Co + Ni + Mn) ratio was imposed by the chemical composition of the oxides. For highly substituted oxides, the refinement procedure is improved by partial mixing between Li^+ from LiO_2-layers and Ni^{2+} from transition metal layers. The driving force for the Li/Ni exchange is the similarity of ionic sizes of Li^+ and Ni^{2+} ions. The concentration dependence of the structural parameters (Table 1) is in accordance with our previous structural data.[8–10]

EPR measurements at 9.23 GHz (X-band) are carried out on an ERS 220/Q spectrometer within the temperature range 85–410 K. The g-factors are established with respect to a Mn^{2+}/ZnS standard. The high-frequency EPR spectra are recorded on a single-pass transmission EPR spectrometer built at the High-Magnetic Field Laboratory, Grenoble, France. The frequencies

Table 1 Lattice parameters (*a* and *c*), oxygen parameter (*z*), Li amount in the transition metal layers (δ) and EPR line width for the signal detected at 9.3 GHz (ΔH_{pp}) for $LiCo_{1-2x}Ni_xMn_xO_2$

Samples	$a \pm 0.0003$ (Å)	$c \pm 0.0014$ (Å)	$z \pm 0.0002$	$\delta \pm 0.004$	$\Delta H_{pp} \pm 0.8$ (mT)
$x = 0.02$	2.8146	14.0641	0.2602	0	—
$x = 0.10$	2.8232	14.1062	0.2609	0	165.0
$x = 0.33$	2.8541	14.2130	0.2603	0.019	141.1
$x = 0.50^a$	2.8788	14.2819	0.2584	0.075	85.0
$x = 0.50^b$	2.8824	14.2792	0.2582	0.081	122.0

[a] Ilmenite-derived oxide. [b] Spinel-derived oxide.

are changed from 95 to 345 GHz using Gunn diodes and their multipliers. The detection of absorption is performed using a bolometer. The recording temperatures are varied from 5 to 300 K applying a variable temperature insert (Oxford Instruments).

Solid-state ^{7}Li NMR spectra were recorded on several Bruker and Agilent NMR spectrometers at different magnetic field strength – 2.35, 4.70, 5.87 and 14.10 T. MAS NMR spectra were recorded either using single pulse excitation ($\sim 30^\circ$) or Hahn echo (1.5–2.5 μs for the 90° pulse) and 0.2 s recycle delay, typically 2000–3000 scans have been acquired. The samples were loaded into zirconia rotors (1.0, 1.3 and 4.0 mm) and spun at different rates. For the fast spinning experiments, 1.0 mm (>50 kHz) and 1.3 mm (20–50 kHz) rotors were used. Chemical shifts are quoted in parts per million, from external LiCl. NMR measurements in the presence of unpaired electron spins introduce generally a line broadening that renders information intractable. However, fast electron spin flips scale all electron nucleus interactions by a factor of $g_e\boldsymbol{B}_0\{S(S+1)\}\mu_B/(3kT)$.[24] The relationship above allows for optimization of the measurement conditions. While the temperature can be increased only by a fractional ratio, the magnetic field can be varied by an order of magnitude. This combined with high 60–100 kHz sample spinning rates enables recording of adequately resolved Li spectra on the more abundant $I = 3/2$ spin isotope (*i.e.* ^{7}Li). Spin relaxation dependency constitutes another factor in the choice of a magnetic field. These considerations are illustrated by representative examples in the following sections. The accuracy in the determination of chemical shifts depends on whether Li is in diamagnetic or paramagnetic environments.

Results and discussion

High-frequency EPR: the oxidation state of nickel and manganese ions

All EPR features concerning the identification of the oxidation state of transition metal ions are summarized in Fig. 2. To facilitate assignment of EPR signals, references for Mn^{4+}, Ni^{3+} and Ni^{2+} ions are taken into account (Fig. 2). In accordance with our previous EPR studies on layered transition metal oxides, the HF-EPR spectrum of isolated Mn^{4+} ions in $LiCoO_2$ consists of an asymmetric signal with $g_\perp = 1.978$ and $g_\parallel = 1.997$, while the single Lorentzian line with an isotropic *g*-value of 2.142 gives rise to the EPR spectrum of Ni^{3+} ions. The HF-EPR spectrum of Ni^{2+} ions contains a broad line with $g = 2.226$.

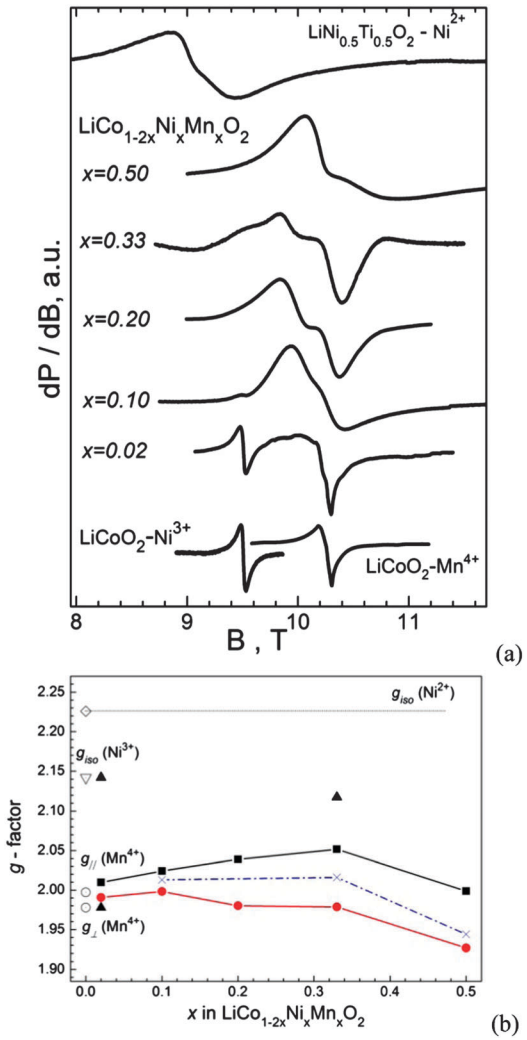

Fig. 2 (a) EPR spectra at 285 GHz of $LiCo_{1-2x}Ni_xMn_xO_2$ with $x = 0.02$, 0.10, 0.2, 0.33 and 0.5. The EPR spectra of Ni^{2+}, Ni^{3+} and Mn^{4+} references are given. (b) The concentration dependence of the *g*-factors for EPR signals. Blue lines correspond to the isotropic *g*-factor determined at 9.23 GHz (X-band region). Spectra are recorded at 100 K.

Comparison of the EPR spectra allows outlining two characteristic EPR features of $LiCo_{1-2x}Ni_xMn_xO_2$, which depend on the Ni and Mn content. For a slightly doped oxide with $x = 0.02$, the EPR spectrum is a convolution between the signals due to isolated Ni^{3+} and Mn^{4+} ions. In addition, weak signals in the range of *g*-values for Mn^{4+} are also visible. After further increase in the total Ni and Mn content, the Ni^{3+} signal is scarcely observed, while the intensity of Mn^{4+} signal increases. At $x \geq 0.1$, the EPR spectrum in the range of *g*-values for Mn^{4+} is split into several components, whose number and *g*-values depend on the Ni and Mn content (Fig. 2b). For $LiCo_{1-2x}Ni_xMn_xO_2$ with $0.1 \leq x \leq 0.5$, two overlapping components dominate in the EPR profile and the concentration dependence of their *g*-factors is given in Fig. 2b. The *g*-factor of the first component slightly decreases, while the *g*-factor of the second one regularly increases reaching a value of 2.05 at the oxide with $x = 0.33$, whereby there is a decrease. For the intermediate composition

x = 0.33, a weak shoulder to the second component becomes visible (Fig. 2a and b). It is worth mentioning that the g-values of all signals are changed without approaching the typical g-value of Ni^{2+} ions (Fig. 2b).

All EPR features permit us to assign the EPR signals to Ni^{3+} and Mn^{4+} ions only. A signal due to Ni^{2+} ions could not be detected in $LiCo_{1-2x}Ni_xMn_xO_2$ oxides even at higher frequency than used. A similar result has already been observed for $LiCoO_2$ slightly doped with Ni and Mn.[9] The lack of EPR signal has been related to the higher magnitude of the zero field splitting parameters for Ni^{2+} in the layered oxide matrix. However, the presence of Ni^{2+} ions is visible in the EPR components due to Mn^{4+} ions. Recently, we have demonstrated that the value of the g-factor of Mn^{4+} increases in a discrete way with the number of Ni^{2+} ions included in its first metal coordination sphere.[8] Hence, the two dominant signals can be associated with Mn^{4+} ions having two distinct configurations: the signal with $g < 2.00$ corresponds to Mn^{4+} ions having as neighbours only diamagnetic Co^{3+} and a similar paramagnetic Mn^{4+}, while the signal with $g > 2.00$ comes from Mn^{4+} whose local environment includes non-similar paramagnetic Ni^{2+} ions in addition to Co^{3+} and Mn^{4+}. By increasing the Ni and Mn content, the increase of the g-value reflects the inclusion of more and more Ni^{2+} ions around Mn^{4+} (Fig. 2b). For the intermediate composition (x = 0.33), three different configurations are detected, while only two become visible for the magnetically concentrated oxide (x = 0.5). This is related to the local non-homogeneous distribution of Co^{3+}, Ni^{2+} and Mn^{4+} ions. The cationic distribution is further complicated for the oxide with x = 0.5 due to the Li^+/Ni^{2+} exchange between layers (Table 1).

Going from high to low microwave frequency (*i.e.* from 285 to 9.23 GHz), all EPR signals merge into one Lorentzian signal with an isotropic g-factor and a line width depending on the Ni and Mn content. Fig. 2 gives the concentration dependence of the isotropic g-factor. It should be noted that the isotropic g-factor determined at 9.23 GHz coincides with the average g-factor of the signals determined at 285 GHz (Fig. 2b). The EPR line width is shown in Table 1. The observed narrowing of the signal with increasing Ni and Mn amount can be explained by the competitive action of dipolar and exchange magnetic interactions. It has been shown that the dipolar interactions lead to an increase of the EPR line width in the paramagnetic system, while the exchange coupling induces a line narrowing.[25,26] The observed concentration trend for the EPR line width demonstrates the dominating role of the magnetic exchange interactions of $LiCo_{1-2x}Ni_xMn_xO_2$.

In conclusion, the oxidation state of paramagnetic nickel ions in $LiCo_{1-2x}Ni_xMn_xO_2$ changes depending on the total Ni and Mn content. For slightly doped $LiCo_{1-2x}Ni_xMn_xO_2$ (x = 0.02), nickel and manganese adopt oxidation states of +3 and +4. The charge compensation of aliovalent Mn^{4+} ions can be achieved either by the occurrence of Li^+ in the transition-metal layers or by the release of Li^+ from the lithium layers. Because all synthesis procedures are accomplished using an excess of the Li salt (about 2%) it is more reasonable to associate the charge compensation of Mn^{4+} ions with an appearance of Li^+ in the transition-metal layers. The Ni^{3+} content reaches a maximum, when x increases from 0 to 0.1, while the Mn^{4+} content increases continuously. Above 2 mol%, Ni^{2+} ions appear in addition to Ni^{3+} ions and lead to a discrete shift in the g-factor of Mn^{4+}. For highly doped oxides ($LiCo_{1-2x}Ni_xMn_xO_2$ with $x \geq 0.10$), nickel and manganese achieve their usual oxidation states of 2^+ and 4^+.

^{7}Li NMR spectra of $LiCo_{0.96}Ni_{0.02}Mn_{0.02}O_2$ containing only Ni^{3+} and Mn^{4+} ions

The knowledge of the oxidation state of nickel and manganese ions serves as guidelines for interpreting ^{7}Li NMR spectra of $LiCo_{1-2x}Ni_xMn_xO_2$. First we start with the composition $LiCo_{0.96}Ni_{0.02}Mn_{0.02}O_2$, where only Ni^{3+} and Mn^{4+} ions are stabilized.

Fig. 3 depicts the ^{7}Li NMR spectra of $LiCo_{0.96}Ni_{0.02}Mn_{0.02}O_2$. The spectrum is dominated by a central resonance at around 0 ppm, which is typical for Li atoms in a diamagnetic environment. Therefore, the strong resonance at −0.2 ppm corresponds to Li nuclei in the LiO_2-layer surrounded only by diamagnetic Co^{3+} ions between two adjacent metal layers (Fig. 1). The weak resonances at around 4 and 8 ppm are compatible with Li in CoO_2-layers with charge compensation of Mn^{4+} ions. Similar downfield shifted resonances have been reported for undoped $LiCoO_2$ obtained in excess of Li.[27,28] In this case, $LiCoO_2$ is capable of accommodating a small excess of Li in the Co layers by the creation of oxygen vacancies, thus leading to $Li_{1+t}Co_{1-t}O_{2-t}$ with $t \approx 0.04$. The overstoichiometric $Li_{1+t}Co_{1-t}O_{2-t}$ gives rise to downfield shifted lines for Li atoms in different environments.[27,28]

The expected effect of paramagnetic nickel and manganese ions is revealed in the low intensity peripheral parts of the spectrum (Fig. 3). The relative intensities of each of the outermost resonances are below 5%. The assignment of these resonances is facilitated by available EPR data, as well as by previous NMR studies on nickel substituted $LiCoO_2$ and monoclinic Li_2MnO_3.[12,29] Thus, the resonances at +112 and −13 ppm can be assigned to Li^+ connected *via* oxygen to Ni^{3+} ions at

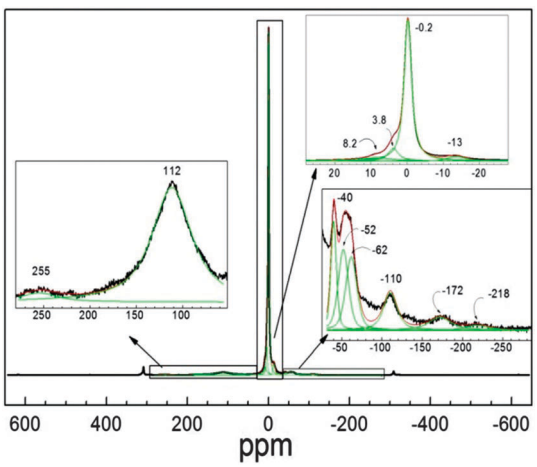

Fig. 3 ^{7}Li NMR spectra of $LiCo_{0.96}Ni_{0.02}Mn_{0.02}O_2$ recorded at 60 kHz MAS. The green lines denote the deconvoluted resonances.

angles of 180° and 90°, respectively (Fig. 1). The signals of the Li^{+}–O^{2-}–Mn^{4+} configurations at 90° and 180° are associated with the lithium resonances at +255 and −52 ppm (Fig. 1 and 3). Since nuclear–electron spin interactions are additive, all additional down and upfield signals can be attributed to combinations of Ni^{3+} and Mn^{4+} ions in the first and second metal positions (90°- and 180°-configuration, respectively, Fig. 1). The resonances at −40 ppm can be associated with the additive effect of three Ni^{3+} ions located in the first position, while the resonances at −110 and −173 come from the 2 and 3Mn^{4+} ions in the second position, respectively. The resonance at −62 ppm can be attributed to Li having 5 Ni^{3+} neighbors in the first position or one Ni^{3+} and one Mn^{4+} in the first and second positions, respectively. The low intensities of the outermost shifted resonances do not allow specifying the exact configuration of Li with respect to the number of nearest Ni^{3+} and Mn^{4+} neighbors. However, the local environment of lithium in $LiCo_{0.96}Ni_{0.02}Mn_{0.02}O_2$ is created mainly by Ni^{3+} or Mn^{4+} ions and less by mixed Ni^{3+} and Mn^{4+} ions. The appearance of distinct Li^{+}–O^{2-}–Ni^{3+} and Li^{+}–O^{2-}–Mn^{4+} configurations suggests that Ni and Mn ions are distributed in such a way to avoid Ni–Mn contact. This result agrees well with the EPR data[9] on the local distribution of isovalent Ni^{3+} and aliovalent Mn^{4+} in $LiCoO_2$.

^{7}Li NMR spectra of intermediate compositions $LiCo_{1-2x}Ni_xMn_xO_2$ ($0.1 \leq x \leq 0.33$)

EPR spectroscopy reveals that upon increasing the total Ni and Mn content ($0.05 < x \leq 0.33$) a variety of paramagnetic ions – Ni^{3+}, Ni^{2+} and Mn^{4+} – are stabilized in $LiCo_{1-2x}Ni_xMn_xO_2$. The benefit of using NMR with fast spinning rates is better illustrated for the oxides having higher number of paramagnetic ions with different content.

Fig. 4 compares the ^{7}Li NMR spectra of $LiCo_{0.8}Ni_{0.1}Mn_{0.1}O_2$ collected at a rotation speed of 14, 50 and 90 kHz. All ^{7}Li NMR spectra include a central line at about 0 ppm surrounded by down- and up-field shifted resonances. The central signal is well reproduced irrespective of the spinning rates and can be decomposed into two components at −1.5 and 2.5 ppm, respectively. In addition the resonance at −14 ppm is also well distinguished. This means that, even at a low spinning rate, partial information concerning the effect of paramagnetic Ni^{3+} ions on the chemical shift of Li can be obtained.

By increasing the spinning rates, the down- and up-field shifted resonances are clearly observed. At 90 kHz, two sets of resonances are distinguished: upfield shifted lines at −14, −25, −50, −75 and −140 ppm and downfield shifted lines at 57, 120 and 225 ppm. As expected the faster the spinning rate, the higher the relative intensities of the outermost resonances observed. Comparison of ^{7}Li spectra of slightly doped compositions $LiCo_{0.96}Ni_{0.02}Mn_{0.02}O_2$ and $LiCo_{0.8}Ni_{0.1}Mn_{0.1}O_2$ shows that resonances due to single 90° Li^{+}–O^{2-}–Ni^{3+}/Mn^{4+} and 180° Li^{+}–O^{2-}–Ni^{3+}/Mn^{4+} configurations are still seen. However, the higher spinning rate (*i.e.* 90 kHz) allows resolving a new resonance at −25 ppm, which is observed for $LiCo_{0.8}Ni_{0.1}Mn_{0.1}O_2$ only. Taking into account the origin of paramagnetic ions

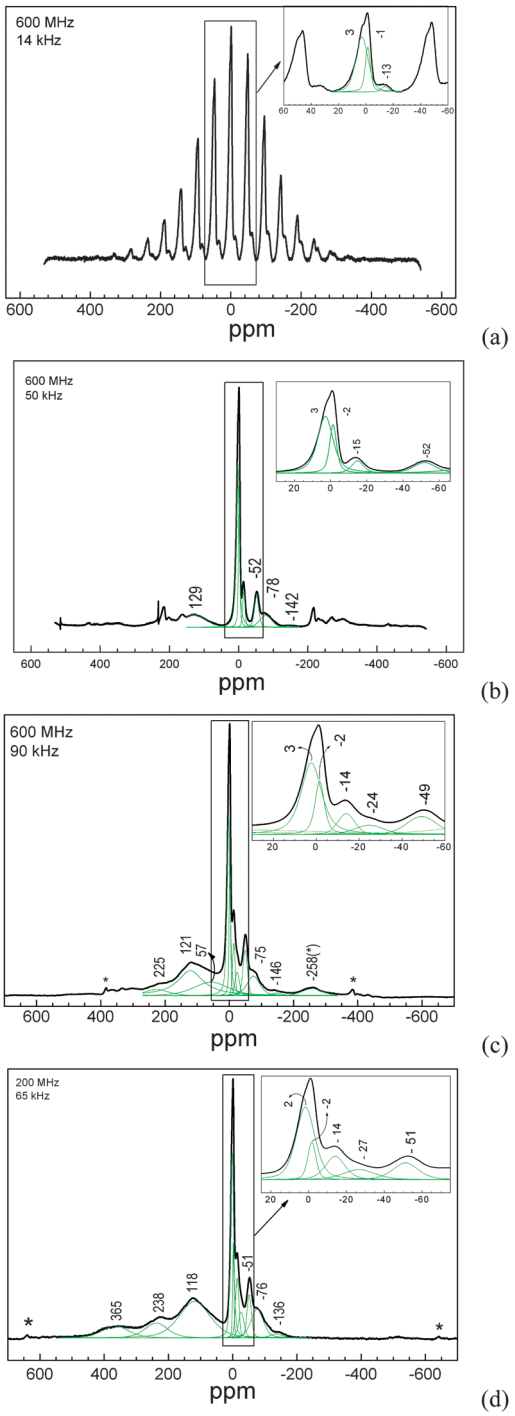

Fig. 4 ^{7}Li NMR spectra of $LiCo_{0.80}Ni_{0.10}Mn_{0.10}O_2$ recorded at a magnetic field strength of 14.10 T and 14 (a), 50 (b) and 90 kHz (c) spinning rate. The ^{7}Li NMR spectrum of $LiCo_{0.80}Ni_{0.10}Mn_{0.10}O_2$ recorded at lower magnetic field (4.70 T) with 65 kHz spinning speed is also given (d). The asterisks denote the spinning side bands.

stabilized in $LiCo_{0.8}Ni_{0.1}Mn_{0.1}O_2$, we can tentatively assign this resonance to Li having one Ni^{2+} ion as a neighbour. The assignment is further supported by the NMR data of Carlier *et al.*[22] on $LiTi_{0.5}Ni_{0.5}O_2$ where only Ni^{2+} is stabilized. Based on the experimental data and DFT calculations,[13,22] it has been

demonstrated that the signal at −30 ppm is due to the effect of Ni^{2+} ions bounded to Li by 90° *via* oxygen. The resonance at +120 ppm can be associated with the effect of Ni^{2+} in the second position. This is the range where the resonance due to 180° Li^{+}–O^{2-}–Ni^{3+} also appears. As in the case of slightly doped $LiCo_{0.96}Ni_{0.02}Mn_{0.02}O_2$, the rest of the outermost resonances at −75, −146 and +57 ppm are a result of the additive effect of Ni^{2+}, Ni^{3+} and Mn^{4+} neighbours on the lithium chemical shift.

As can be expected for paramagnetic oxides, the magnetic field strength also affects the ^{7}Li NMR profile. Fig. 4 gives the ^{7}Li NMR spectra recorded at lower magnetic field (4.7 T) at a 65 kHz spinning rate. In general, the ^{7}Li NMR spectra display the same features at low and high-fields: intensive double resonance at 0 ppm surrounded by low-intensive outermost resonances. It should be noted that observation of the signal due to neighbouring Ni^{2+} ions is achieved at a rotation speed of 65 kHz at lower magnetic field, while a spinning rate of 90 kHz is needed to observe the same resonance at higher magnetic field (Fig. 4). In addition, there is a new downfield shifted resonance at +365 ppm. This signal can be attributed to the additive effect of one Mn^{4+} at a first position and one Ni^{2+} at a second position on the chemical shift of Li. Interestingly, the magnetic field strength influences more significantly the observation of lithium resonances due to the effect of Ni^{2+} in comparison with that due to the effect of Mn^{4+} ions.

Comparison of the spectra recorded at different magnetic fields shows that a better resolution is achieved if a lower magnetic field is applied. This feature is consistent with the relaxation properties of paramagnetic systems. It has been shown that the Li line width in paramagnetic oxides and poly-anion compounds is mainly governed by the spin–lattice relaxation of the electrons to which the nucleus is coupled.[30] The relaxation depends on the magnetic field strength because the population difference of the energy spin levels increases with the magnetic field applied.[31] In this context, lower magnetic fields are more suitable for probing smaller distances while higher fields are more suited for longer distances.[31] As a consequence of the paramagnetic relaxation, the spin state of transition metal ions is a key factor determining the spectral resolution in ^{7}Li NMR spectra. A simple illustration is the measured line width of Li surrounded by Ni^{3+}, Mn^{4+} and Ni^{2+} ions having spin states of 1/2, 3/2 and 1. In the spectrum registered at 14.10 T with a spinning rate of 90 kHz, the ^{7}Li line width amounts from 2.2 kHz, 3.7 kHz to 3.9 kHz, respectively.

The ^{7}Li NMR spectrum of intermediate composition $LiCo_{0.33}Ni_{0.33}Mn_{0.33}O_2$ is shown in Fig. 5. The spectrum displays a broad envelope, where two resonances with a centre of gravity at 575 and 326 ppm can be deconvoluted. It is worth to mention that, even at the highest spinning rate used, the ^{7}Li spectrum of the intermediate composition remains featureless in comparison with that for the magnetically diluted oxide $LiCo_{0.8}Ni_{0.1}Mn_{0.1}O_2$ (Fig. 4). In this case, the EPR data allow explaining the ^{7}Li NMR spectrum. For x = 0.33, HF-EPR reveals three distinct configurations of Mn^{4+} inside the transition metal layer: Mn^{4+} surrounded only by Co^{3+} and Mn^{4+} ions and Mn^{4+} ions having different number of Co^{3+}, Mn^{3+} and Ni^{2+} ions as neighbours. Thus the resonance with a centre of gravity at 575 ppm can be attributed to Li having $2Mn^{4+}$ neighbours in the first position, while $1Mn^{4+}$ and $1Ni^{2+}$ in the first and second position should be responsible for the appearance of the resonance at 326 ppm. On the other hand, the observation of downfield shifted resonances gives evidence that Mn^{4+} in the first position has a dominant role in the ^{7}Li NMR spectra.

^{7}Li NMR spectra of $LiNi_{0.5}Mn_{0.5}O_2$ containing Ni^{2+} and Mn^{4+}

Further increase of the total Ni and Mn content leads to a large downfield shift of the centre of gravity of the ^{7}Li resonance (Fig. 5 and 6). In comparison with the intermediate composition $LiCo_{0.33}Ni_{0.33}Mn_{0.33}O_2$, the ^{7}Li spectrum of the end composition $LiNi_{0.5}Mn_{0.5}O_2$, where only Ni^{2+} and Mn^{4+} co-exist, is better resolved (Fig. 6). The resolution enhancement for the paramagnetic $LiNi_{0.5}Mn_{0.5}O_2$ is related to the magnetic exchange interactions between Ni^{2+} and Mn^{4+} ions in addition to the dipolar Ni^{2+}–Mn^{4+} interactions. An analogous mechanism of line narrowing is also seen in the EPR signal (Table 1).

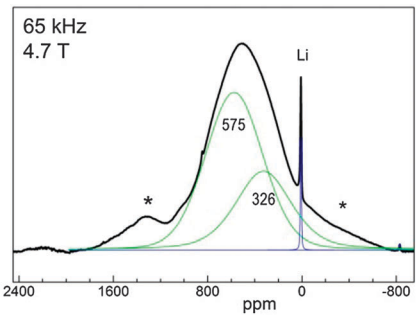

Fig. 5 ^{7}Li NMR spectrum of $LiCo_{0.33}Ni_{0.33}Mn_{0.3}O_2$ recorded at a magnetic field of 4.70 T with a 65 kHz spinning rate. The resonance due to impurity of diamagnetic lithium salt is denoted by Li.

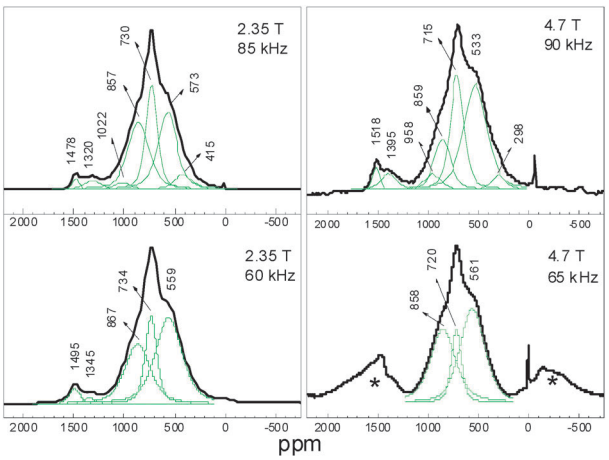

Fig. 6 ^{7}Li NMR spectra of ex-ilmenite $LiNi_{0.5}Mn_{0.5}O_2$ recorded at 2.35 T and 4.70 T with various spinning rates. The asterisks denote the spinning side bands.

Table 2 Peak position (δ, ppm), line width (Θ, kHz) and relative intensity (I, %) of the deconvoluted lines in ^{7}Li NMR spectra of ex-ilmenite and ex-spinel $LiNi_{0.5}Mn_{0.5}O_2$ (LNMO). The spectra are recorded at low and high magnetic fields (MF) with ultrafast spinning rates (SR)

Ex-ilmenite LNMO			Ex-ilmenite LNMO			Ex-spinel LNMO		
MF: 4.70 T			MF: 2.35 T			MF: 2.35 T		
SR: 90 kHz			SR: 85 kHz			SR: 86.2 kHz		
δ (ppm)	Θ (kHz)	I (%)	δ (ppm)	Θ (kHz)	I (%)	δ (ppm)	Θ (kHz)	I (%)
298	14.4	3.9	451	9.1	6.1	434	15.5	8.9
533	21.2	42.5	573	8.6	31.4			
715	12.6	27.6	730	5.1	25.2	690	17.9	85.7
859	15.1	14.4	857	9.5	29.9			
958	15.9	4.7	1022	7.8	2.7			
1395	15.3	4.4	1320	8.1	3.2	1355	7.6	4.6
1518	6.4	2.5	1478	3.1	1.5	1569	5.4	0.7

Fig. 6 compares the effect of spinning rates and magnetic field strength on the ^{7}Li NMR profile. For simplicity, this figure gives only the most representative spectra recorded at two selected spinning rates of 60 and 90 kHz and at low and high magnetic fields. A close inspection reveals that the ^{7}Li NMR spectrum consists of several download shifted resonances, whose number and relative intensities depend on the spinning rate and the magnetic field strength. Table 2 shows the positions, line widths and relative intensities of the deconvoluted signals. It appears that the ^{7}Li NMR profile becomes constant when 90 kHz is used. At this speed, the eight overlapping resonances are resolved (Table 2), *ca.* 94% of them cover the range between 300 and 1000 ppm and less than 6% encompass the range of 1350–1500 ppm. The important feature is that the resonances at 720 and 1500 ppm exhibit a lower line width in comparison with other resonances. The observation of distinct chemical shifts of Li in $LiNi_{0.5}Mn_{0.5}O_2$ implies that the local lithium environment is quantized in respect of the number of Ni^{2+} and Mn^{4+} neighbors.

To assign the observed chemical shifts, we used monoclinic Li_2MnO_3 as a reference system for 90° and 180° Li^+–O^{2-}–Mn^{4+} configurations. In comparison with $LiNi_{0.5}Mn_{0.5}O_2$, Li_2MnO_3 has a structure composed of lithium and mixed $Li_{1/3}Mn_{2/3}$-layers. Inside $Li_{1/3}Mn_{2/3}$-layers, Li^+ and Mn^{4+} are ordered by creating two distinct positions (α,β-sites):[32] Li^+ occupies preferentially the α-site and is surrounded by $6Mn^{4+}$ neighbors, while Mn^{4+} resides at the β-site and has $4Mn^{4+}$ and $2Li^+$ ions as first neighbors. Previous NMR studies on monoclinic Li_2MnO_3 have shown that $6Mn^{4+}$ neighbors in the 90° configurations cause a total chemical shift for Li of 1511 ppm.[33] In the lithium layers, there are two lithium positions whose local structures are built by $4Mn^{4+}$ with an average bond angle Li^+–O^{2-}–Mn^{4+} of 92–93°, $4Mn^{4+}$ with an average bond angle Li^+–O^{2-}–Mn^{4+} of 171–172° and $4Li^+$ ions. The Mn^{4+} neighbors are responsible for a chemical shift in the range of 759–775 ppm. During partial replacement of Mn^{4+} by Ni^{2+}, it has been found that two sets of lithium chemical shifts move upfield: from 1511 to 1341 and from 737 to 587 ppm for $Li[Li_{1/9}Ni_{1/3}Mn_{5/9}]O_2$.[29] This result outlines once again that Mn^{4+} ions produce a larger chemical shift for Li in comparison with Ni^{2+} ions.

Based on these NMR studies, we can attribute the resonances between 1300 and 1500 ppm to Li nuclei surrounded mainly by Mn^{4+} in 90°-configuration. This configuration with a relative intensity less than 6% mimics the local environment of Li in the $Li_{1/3}Mn_{2/3}$-layer of monoclinic Li_2MnO_3. Therefore, one can associate the resonances at 1300–1500 ppm with Li located in the transition metal layers (Fig. 1). The partial mixing of Li^+ and Ni^{2+} ions between the layers is a specific feature of layered lithium transition metal oxides which results from their close ionic radii. For $LiNi_{0.5}Mn_{0.5}O_2$, the amount of Li residing in the transition metal layers is shown to be 7.5% (Table 1) as evaluated from the Rietveld analysis of XRD patterns.

The second set of resonances located between 300 and 1000 ppm can be related to Li nuclei in the lithium layers having Ni^{2+} and Mn^{4+} neighbors distributed over the two 90 and 180° positions. The resonance at 715 ppm matches the chemical shift of Li in the Li-layers of monoclinic Li_2MnO_3, which enables its assignment to Li having only Mn^{4+} and Li^+ as neighbors. The insertion of Ni^{2+} in close proximity to Li is, most probably, responsible for the observed distinct resonances at 400–600 and 800–1000 ppm. Because Mn^{4+} coupled to Li^+ by 90° causes a large lithium chemical shift, the progressive shift of the resonances from 300 to 1000 ppm reveals a smooth increase of the number of Mn^{4+} neighbors with respect to the number of Ni^{2+} ions.

Correlation of the local structure with the electrochemical properties of $LiNi_{0.5}Mn_{0.5}O_2$

The next important question is whether the cationic distribution in $LiNi_{0.5}Mn_{0.5}O_2$ is sensitive towards the synthesis procedure. Recently, we demonstrated that $LiNi_{0.5}Mn_{0.5}O_2$ delivers high capacity with good retention only when $LiNi_{0.5}Mn_{0.5}O_2$ is prepared by a solid state reaction between Ni and Mn oxides with an ilmenite-type structure and lithium hydroxide.[11] The replacement of ilmenite $NiMnO_3$ with a spinel precursor $Ni_{1.5}Mn_{1.5}O_4$ leads to formation of $LiNi_{0.5}Mn_{0.5}O_2$ with inferior electrochemical properties.[11] In the potential range 2.0–4.6 V, ex-ilmenite $LiNi_{0.5}Mn_{0.5}O_2$ delivers a capacity of 200 mA h g^{-1} with a capacity retention of 98% after 35 cycles in model lithium cells, while 195 mA h g^{-1} with a capacity retention of 90% is reached in the potential range of 2.5–4.8 V for ex-spinel $LiNi_{0.5}Mn_{0.5}O_2$.[11] At a first glance, the effect of the precursor used remains unclear since both ilmenite- and spinel-derived

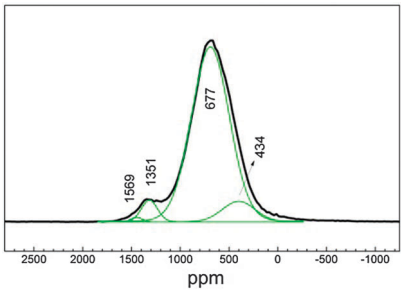

Fig. 7 ^{7}Li NMR spectra of spinel-derived $LiNi_{0.5}Mn_{0.5}O_2$ at 2.35 T with a spinning rate of 86.2 kHz.

oxides $LiNi_{0.5}Mn_{0.5}O_2$ are characterized by the same long-range crystal structure (Table 1) and close particle dimensions (about 140 nm).[11]

^{7}Li NMR spectra of both samples are clearly differentiated by the centre of gravity of the broad resonance and the number of deconvoluted signals (Fig. 6 and 7). The comparison gives evidence that, for the spinel-derived oxide $LiNi_{0.5}Mn_{0.5}O_2$, the centre of gravity shifts from 730 to 690 ppm and the number of resolved lines is reduced from 7 to 4 (Fig. 6 and 7). In the same order, the line width of the resonances seems to be 2 to 3 times higher (Table 2). Only the resonances in the range of 1300–1500 ppm remain unchanged for both samples. The lack of any influence on these resonances of the method of synthesis is in good agreement with the amount of Li in the transition metal layers determined by XRD analysis (Table 1). Since Ni^{2+} ions induce a much smaller chemical shift for Li in comparison with Mn^{4+}, the observed shift in the centre of gravity for spinel-derived $LiNi_{0.5}Mn_{0.5}O_2$ reveals accumulation of a higher number of nickel ions around Li. In order to check this supposition, we compare the NMR results with our previous EPR data on the local structure of Mn^{4+} ions. Based on the relationship between the EPR line width and the Ni-to-Mn ratio, we estimated the local Ni-to-Mn ratio as a measure of Ni and Mn distribution in the transition metal layers:[10] the values are 1.06 and 1.42 for ex-ilmenite and ex-spinel $LiNi_{0.5}Mn_{0.5}O_2$, respectively. (For the sake of comparison, the Ni-to-Mn ratio determined from chemical analysis is 0.96 and 0.99, respectively). This result indicates that Ni^{2+} and Mn^{4+} are non-randomly distributed inside the transition metal layers and the extent of local ordering is higher for the oxide $LiNi_{0.5}Mn_{0.5}O_2$ obtained from the spinel precursor.[10]

Conclusions

Acquisition of EPR spectra at high frequency permits us to identify the oxidation states of transition metal ions in several $LiCo_{1-2x}Ni_xMn_xO_2$ compositions. While Co and Mn ions adopt the oxidation states of +3 and +4 in the whole concentration range, the oxidation state of nickel ions is transformed from +3 to +2 upon increasing the total Ni and Mn content. The information on the oxidation state of transition metal ions serves as guidelines for the interpretation of Li NMR spectra.

The oxide with $x = 0.02$ is regarded as a model system for evaluating the effect of Ni^{3+} and Mn^{4+} on the chemical shift of Li^+. The resonances at +112 and −13 ppm are attributed to Li^+ coupled to Ni^{3+} ions by 180° and 90° *via* oxygen, while the contribution of 90° and 180° Li^+–O^{2-}–Mn^{4+} configurations is associated with lithium resonances at +255 and −52 ppm. Both EPR and NMR spectra show that isovalent Ni^{3+} and aliovalent Mn^{4+} are distributed in CoO_2-layers in such a way to avoid Ni–Mn contact.

When x increases to 0.1, the Ni^{3+} content reaches a maximum, while the Mn^{4+} content increases continuously. Above 2 mol%, Ni^{2+} ions start to appear in addition to Ni^{3+} ions and lead to a discrete increase in the g-factor of Mn^{4+}. The presence of Ni^{2+} is detected *via* a Li chemical shift at −25 and +120 ppm depending on the bond angle Li^+–O^{2-}–Ni^{2+}. The magnetic field strength has a more pronounced influence on lithium sites close to Ni^{2+} than on those in the neighbourhood of Mn^{4+} ions. As a result, the ^{7}Li NMR spectra, especially for $x = 0.33$, are dominated by Mn^{4+} in the first position.

The observation of distinct chemical shifts of Li in $LiNi_{0.5}Mn_{0.5}O_2$ implies that the local lithium environment could be quantified in respect of the number of Ni^{2+} and Mn^{4+} neighbors. Two sets of Li chemical shift are observed: between 1300 and 1500 ppm and between 300 and 1000 ppm. The progressive downfield shift from 300 to 1000 ppm identifies the smooth increase of the number of Mn^{4+} neighbors with respect to the number of Ni^{2+} ions. The partial mixing of Li^+ and Ni^{2+} ions between the layers is a specific feature of layered lithium transition metal oxides that is manifested by a downfield chemical shift in the region of 1300–1500 ppm. It is worth mentioning that to the best of our knowledge this is the first example of observation of well resolved lithium resonances due to the use of ultrafast spinning rates.

Both EPR and NMR techniques demonstrate that Ni^{2+} and Mn^{4+} are non-randomly distributed around Li^+ and the extent of local ordering depends on the method of synthesis. From an electrochemical point of view, the composition with lower extent of local Ni^{2+}/Mn^{4+} ordering would be more suitable as a cathode material for lithium ion batteries.

The consistency between EPR and NMR represents a valuable methodology for analysis of the local structure and its impact on the electrochemical properties of lithium transition metal oxides. This spectroscopic approach could be extended beyond the electrode materials for lithium ion batteries since its goal is a rational design of material properties.

Acknowledgements

The authors are grateful for the financial support from National Centre for New Materials UNION (Contract No DCVP-02/2/2009). Additional financial support from the Bulgarian National Science Fund – Projects DRNF-02-13/2009 is gratefully acknowledged. A.S. would also acknowledge TUT Base financing, NMR Institute, Estonian Science Foundation, Research Council and Academy of Sciences for support.

Notes and references

1 E. Zhecheva, R. Stoyanova, R. Alcántara, P. Lavela and J. L. Tirado, *Pure Appl. Chem.*, 2002, **74**, 1885.
2 M. M. Thackeray, C. S. Johnson, J. T. Vaughey, N. Li and S. A. Hackney, *J. Mater. Chem.*, 2005, **15**, 2257.
3 Z. Lu, D. D. MacNeil and J. R. Dahn, *Electrochem. Solid-State Lett.*, 2001, **4**, A191.
4 B. L. Ellis, K. T. Lee and L. F. Nazar, *Chem. Mater.*, 2010, **22**, 691.
5 J. Krzystek, A. Ozarowski and J. Telser, *Coord. Chem. Rev.*, 2006, **250**, 2308.

6 R. Stoyanova, E. Zhecheva, R. Alcántara and J. L. Tirado, *J. Mater. Chem.*, 2006, **16**, 359.
7 R. Stoyanova, E. Zhecheva and S. Vassilev, *J. Solid State Chem.*, 2006, **179**, 378.
8 E. Shinova, R. Stoyanova, E. Zhecheva, G. F. Ortiz, P. Lavela and J. L. Tirado, *Solid State Ionics*, 2008, **179**, 2198.
9 R. Stoyanova, A.-L. Barra, M. Yoncheva, E. Zhecheva, E. Shinova, P. Tzvetkova and Sv. Simova, *Inorg. Chem.*, 2010, **49**, 1932.
10 M. Yoncheva, R. Stoyanova, E. Zhecheva, R. Alcántara and J. L. Tirado, *J. Alloys Compd.*, 2009, **475**, 96.
11 M. Yoncheva, R. Stoyanova, E. Zhecheva, R. Alcántara, G. Ortiz and J. L. Tirado, *Electrochim. Acta*, 2009, **54**, 1694.
12 C. Marichal, J. Hirschinger, P. Granger, M. Menetrier, A. Rougier and C. Delmas, *Inorg. Chem.*, 1995, **34**, 1773.
13 D. Carlier, M. Ménétrier, C. P. Grey, C. Delmas and G. Ceder, *Phys. Rev. B: Condens. Matter Mater. Phys.*, 2003, **67**, 174103.
14 C. Chazel, M. Ménétrier, D. Carlier, L. Croguennec and C. Delmas, *Chem. Mater.*, 2007, **19**, 4166.
15 C. P. Grey and N. Dupré, *Chem. Rev.*, 2004, **14**, 4493.
16 W. S. Yoon, S. Iannopollo, C. P. Grey, D. Carlier, J. Gorman, J. Reed and G. Ceder, *Electrochem. Solid-State Lett.*, 2004, **7**, A167.
17 D. Zeng, J. Cabana, J. Bréger, W.-S. Yoon and C. P. Grey, *Chem. Mater.*, 2007, **19**, 6277.
18 L. S. Cahill, S.-C. Yin, A. Samoson, I. Heinmaa, L. F. Nazar and G. R. Gward, *Chem. Mater.*, 2005, **17**, 6560.
19 M. Carewska, S. Scaccia, F. Croce, S. Arumugam, Y. Wang and S. Greenbaum, *Solid State Ionics*, 1997, **93**, 227.
20 G. Pintacuda and G. Kervern, *Top. Curr. Chem.*, 2013, **335**, 157.
21 D. S. Middlemiss, A. J. Ilott, R. J. Clément, F. C. Strobridge and C. P. Grey, *Chem. Mater.*, 2013, **25**, 1723.
22 D. Carlier, K. Kang, G. Ceder, W. S. Yoon, C. P. Grey, 203rd ECS Meeting, Paris, France, April 27–May 2, 2003.
23 J. Rodrigues-Carvajal, Satellite Meeting on Powder Diffraction of the XV Congress of the IUCr, 1990, p. 127.
24 A. Nayeem and J. P. Yesnowski, *J. Chem. Phys.*, 1988, **89**, 4600.
25 P. W. Anderson and P. R. Weiss, *Rev. Mod. Phys.*, 1953, **25**, 269.
26 T. Morya, *Prog. Theor. Phys.*, 1956, **16**, 23.
27 S. Levasseur, M. Ménétrier, Y. Shao-Horn, L. Gautier, A. Audemer, G. Demazeau, A. Largeteau and C. Delmas, *Chem. Mater.*, 2003, **15**, 348.
28 M. Ménétrier, D. Carlier, M. Blangero and C. Delmas, *Electrochem. Solid-State Lett.*, 2008, **11**, A179.
29 M. Jiang, B. Key, Y. S. Meng and C. P. Grey, *Chem. Mater.*, 2009, **21**, 2733.
30 L. J. M. Davis, I. Heinmaa, B. L. Ellis, L. F. Nazar and G. R. Goward, *Phys. Chem. Chem. Phys.*, 2011, **13**, 5171.
31 S. Ishihara, K. Deguchi, H. Sato, M. Takegawa, E. Nii, S. Ohki, K. Hashi, M. Tansho, T. Shimizu, K. Ariga, J. Labuta, P. Sahoo, Y. Yamauchi, J. P. Hill, N. Iyi and R. Sasai, *RSC Adv.*, 2013, **3**, 19857.
32 P. Strobel and B. Lambert-Andron, *J. Solid State Chem.*, 1998, **75**, 90.
33 J. Bréger, M. Jiang, N. Dupre, Y. S. Meng, Y. Shao-Horn, G. Ceder and C. P. Grey, *J. Solid State Chem.*, 2005, **178**, 2575.